Divergent granulopoiesis at extramedullary sites safeguards host defense

Carlos Silvestre-Roig[1]*, Raphael Chevre[1], Merieme Farjia[1], Alexander Bender[1], Lina M. Vöcking[1], Mathis Richter[1], Ali Hageb[1], , Vincent Suerdiek[1], Francisco J. Arenas Cerro[2,3], Quinte Braster[4], Mauricio Guzman[5], Jordi Sintes[6], Samriti Sharma[7], Patricia Lemnitzer[8], Claudia Tulotta[1], Yvonne Börgeling[9], Andrea Herrero-Cervera[1], Hannah Flueter[1], Sara Noemi Reinartz Groba[1], David Ahern[10], Collins Osei-Sarpong[1], Ralf Zimmer[11], Noelia Alonso-Gonzalez[12], Eduardo Ortega[2,3], Stefan Lienenklaus[13], Ulrich Kalinke[14], Stephan Ludwig[9], Daniel R. Engel[15], Frank Rosenbauer[16], Claudia Monaco[10], Petra Dersch[7], Artur Kibler[17], Andrea Cerutti[5,18,19], Triantafyllos Chavakis[20], Rui Benedito[20,21], Andres Hidalgo[22], Jadwiga Jablonska[23], Miguel Palomino-Segura[2,3], Oliver Soehnlein[1]*.

[1]Institute of Experimental Pathology (ExPat), Center for Molecular Biology of Inflammation (ZMBE), University of Münster, Münster, Germany
[2]**Immunophysiology Research Group, Instituto Universitario de Investigación Biosanitaria de Extremadura (INUBE), University of Extremadura, Badajoz, Spain.**
[3]Immunophysiology Research Group, Physiology Department, Faculty of Sciences, University of Extremadura, Badajoz, Spain.
[4]Biolegend, The Netherlands
[5]Translational Clinical Research Program, Hospital del Mar Medical Research Institute (IMIM), Barcelona, Spain
[6]Roche Diagnostics, Spain
[7]Institute of Infectiology, Center for Molecular Biology of Inflammation (ZMBE), University of Münster, Münster, Germany
[8]Department of Hematology, Oncology and Cancer Immunology, Charité - Universitätsmedizin Berlin, Corporate Member of Freie Universität Berlin, Germany
[9]Institute of Molecular Virology, Centre for Molecular Biology of Inflammation, University of Münster, Muenster, Germany.
[10]Kennedy Institute of Rheumatology, Nuffield Department of Orthopedics, Rheumatology and Musculoskeletal Sciences, University of Oxford, United Kingdom
[11]Department of Informatics, Ludwig-Maximilians University, Munich, Germany
[12]Institute of Immunology, University of Muenster, Muenster, Germany
[13]Institute of Laboratory Animal Science, Hannover Medical School, 30625 Hannover, NI, Germany.
[14]Institute for Experimental Infection Research, TWINCORE, Centre for Experimental and Clinical Infection Research, a joint venture between the Helmholtz Centre for Infection Research [HZI], Braunschweig, and the Hannover Medical School [MHH], 30625, Hannover, Germany.
[15]Institute for Experimental Immunology and Imaging, Department of Immunodynamics, University Hospital Essen, Essen, Germany
[16]Institute of Molecular Tumor Biology, University of Münster, Münster, Germany.
[17]Precision Immunology Institute, Icahn School of Medicine at Mount Sinai, New York, NY, USA.
[18]Catalan Institute for Research and Advanced Studies (ICREA), Barcelona, Spain
[19]Institute for Clinical Chemistry and Laboratory Medicine, University Hospital and Faculty of Medicine, Technische Universität Dresden, Dresden, Germany
[20]Molecular Genetics of Angiogenesis Group, Centro Nacional de Investigaciones Cardiovasculares (CNIC), Madrid, Spain.
[2]1Department of Functional Genetics, Max Planck Institute for Molecular Biomedicine, Münster, Germany
[22]Department of Immunobiology, Program of Vascular Biology and Therapeutics, Yale University, New Haven, CT, USA
[23]Department of Otorhinolaryngology, University Hospital Essen, University Duisburg-Essen, Germany
* Correspondence should be addressed to CSR or OS: silvestre.roig@uni-muenster.de or soehnlein@uni-muenster.de

Abstract

Extramedullary organs such as the spleen can assume granulopoiesis as a supportive mechanism to cope with the demands during persistent inflammation. However, the quantitative output of extramedullary granulopoiesis is limited, thus raising the question if the spleen in fact provides neutrophils of a qualitative difference rather than merely contributing to neutrophil numbers. Here we report splenic stress granulopoiesis with distinct production and differentiation trajectories. Myeloid progenitors in the spleen engage in accelerated production of neutrophils with an immature phenotype. Yet, neutrophils generated during persistent stress granulopoiesis are fully competent to exert antimicrobial functions and are necessary to contain bacterial invasion. Activation of type I interferon signaling in the spleen is required for splenic neutrophil priming and its loss impairs host defense. Thus, the spleen provides an immunological environment for stress-induced rapid production and priming of highly active neutrophils to meet the demands during infection.

Introduction

Neutrophils are the major constituent of the innate arm of the host response against invading pathogens. Production and mobilization of neutrophils are tightly regulated processes that control the daily level of circulating neutrophils during steady state (*1*). However, this precise regulation is dramatically altered during acute inflammation leading to a massive discharge of neutrophils. Persistence of the inflammatory signals in not rapidly cleared infections initiates a program of emergency granulopoiesis facilitating the recovery of the emptied neutrophil bone marrow pool and maintaining the supply of neutrophils in the circulation with distinct levels of maturation (*1, 2*). Under such conditions, hematopoietic stem and progenitor cells (HSPCs) and myeloid progenitors can be mobilized to the circulation and engraft in secondary organs such as the spleen or liver in a process termed extramedullary hematopoiesis (EMH) (*3*). In mice, this process occurs not only during infection (*4, 5*) but extends to other states of sustained inflammation such as cardiovascular disease (*6, 7*) or cancer (*8*). Similarly, counts of circulating hematopoietic stem cells (HSCs) and progenitors increase in individuals suffering from such pathologies. EMH permits outsourcing neutrophil production to secondary organs for the bone marrow to compensate for a deficit in physical space; however, the limited neutrophil output by extramedullary production is at odds with this concept.

Neutrophil functionality can be shaped across their production and differentiation pipeline (*9*), a process that can be beneficial for the host upon inflammatory pressure. Thus, we here hypothesize that stress-induced granulopoiesis independent of the bone marrow arises as a host mechanism to meet qualitative rather than quantitative neutrophil output in response to lasting inflammatory insults. Here, we investigate the importance of extramedullary granulopoiesis as a supportive mechanism for neutrophil production under inflammatory stress. Using epigenomic and functional profiling of neutrophils across the differentiation tree in the bone marrow and spleen, we show that the spleen serves as a site that rapidly produces neutrophils with enhanced antimicrobial function. We demonstrate that type I interferon signaling primes neutrophil progenitors for express differentiation into neutrophils which are prematurely released into the circulation. Functional analysis demonstrated that this premature subpopulation exhibits fully competent effector functions facilitating microbe elimination.

Results

Alternative granulopoiesis emerges from extramedullary production

To comprehensively profile emergency granulopoiesis in the spleen, we mapped the hematopoietic differentiation dynamics from hematopoietic stem and progenitor cells to differentiated immature and mature neutrophils across chronic conditions that alter neutrophil production by flow cytometry (**Figure 1, Extended Figure 1**). C57BL6/J mice subjected to models of melanoma, repeated lipopolysaccharide (LPS) administration, aging, and hypercholesterolemia were profiled from $Lin^{-}Sca1^{+}cKit^{+}$ (LSKs) cells all the way to immature (immNEU) and mature (matNEU) neutrophils within the bone marrow and the spleen (**Figure 1A/B, Extended Figure 1B-G**). Splenic myelopoiesis generated a strong neutrophil-biased hematopoiesis with a striking expansion of preNEUs in absolute counts and the differentiation to immNEU and matNEU respective to spleen-resident cells found in steady-state. This expansion of neutrophil progenitors and descendants in the spleen mimicked bone marrow granulopoiesis under steady-state (**Figure 1A, Extended Figure 1D**); importantly, granulopoiesis in the bone marrow was only mildly affected during stress conditions studied here (**Figure 1B, Extended Figure 1D**). Our results suggest that - under a variety of persistent challenges - the spleen engages in active granulopoiesis with expansion of neutrophil progenitors and elevated production of neutrophils peaking at the immature stage. To simplify and harmonize these models we made use of a model of myeloablation (***10***) based on treatment with one single dose of cyclophosphamide (CPM) followed by repeated administration of the CXCR4 antagonist (AMD3100, model of CPM/AMD); this model recapitulated the commonality of stress-induced granulopoiesis in the spleen in all other models with similar proportions and numbers (**Figure 1C, 1D, Extended Figure 1E-G**) while omitting the inflammatory component associated to these. We hence focused on this reductionist model to detail neutrophil production and differentiation at single-cell resolution. Spectral flow cytometry analysis using an antibody panel of 19 markers was used to generate high-dimensional analysis of neutrophil differentiation dynamics employing the PHATE algorithm (***11***) (**Figure 1E**). These analyses confirmed that splenic granulopoiesis is associated with a strong expansion of neutrophil progenitors and immature neutrophils and revealed elevated blood counts of immNEU in these mice. To further detail splenic granulopoiesis at a transcriptomic level, we performed scRNA-seq profiling of myeloid progenitors, neutrophil-committed progenitors (proNEU-preNEU), immature and mature neutrophils. $Gr1^{+}CD115^{+}$ (including both neutrophils and monocytes) and $cKit^{+}$ cells from blood, bone marrow and spleen in control or CPM/AMD-treated mice were FACS-sorted (**Extended Figure 2A**) and processed for scRNA-seq analysis. After quality control, a total of 14,042 cells were used for analysis. We next performed unbiased dimensionality reduction and unsupervised clustering on an aggregate of blood, bone marrow and splenic cells from both control and CPM/AMD treatment (**Extended Figure 2B**). Cell annotation using published cell-specific marker datasets and data curation based on differential expression analysis among identified clusters revealed populations of myeloid progenitors, neutrophil-committed progenitors, immature and mature neutrophils, monocytes, NK-cells, and a subpopulation of dendritic-like cells (**Extended Figure 2B**, lower panel). Analysis of cell proportions recapitulated the results observed in our flow cytometry experiments, *i.e.*, a significant expansion of the neutrophil compartment at the expense of monocytic lineages (**Extended Figure 2C**). We next clustered neutrophil progenitors and

differentiated neutrophils to analyze neutrophil differentiation pathways in both bone marrow and spleen and their end-stage in the blood (**Extended Figure 2D, 2E**). Analysis of neutrophil subpopulations showed that mature neutrophils dominated the blood compartment in steady-state conditions while immature neutrophils emerged upon EMH (**Figure 1F**) thus confirming our flow cytometry analyses (**Figure 1E**). Interestingly, while the bone marrow remained largely unaltered during EMH, a marked increase in immature neutrophils was found in the spleen. Intriguingly, while the differentiation from the immature to mature neutrophils was continuous in the bone marrow, it was interrupted in the spleen suggesting alterations in the differentiation path and a potential release to the circulation at a premature stage (arrows in **Figures 1E, F**). Importantly, such discontinuous granulopoiesis was also observed in other chronic stress models such as in hypercholesterolemia (**Extended Figure 2F**) and during tumor development (**Extended Figure 2G**). Notably, a significant increase in this subpopulation of immature neutrophils is observed in the blood (**Figure 1E, F**), thus suggesting a rapid mobilization from their splenic niche. Collectively, while minor changes are observed in the bone marrow, the spleen assumes an alternative and interrupted granulopoiesis under inflammatory stress to produce neutrophils whose differentiation stops at a premature stage before being mobilized to the circulation.

Splenic granulopoiesis provides the circulation with immature neutrophils

We next sought to determine the contribution of splenic granulopoiesis to circulating neutrophil populations. Herein, we performed mass cytometry analysis using a panel of 35 markers on blood, bone marrow, and spleen leukocytes in vehicle and CPM/AMD-treated mice (**Figure 2A**). After normalization, high-dimensionality reduction and unbiased clustering, we annotated the leukocytes based on their expression of lineage markers (**Extended Figure 3A**). Next, we focused on $Ly6G^+$ neutrophils and performed unbiased clustering on selected cells, identifying 15 metaclusters (**Figure 2A, Extended Figure 3B**) with differential enrichment across organs and conditions (**Extended Figure 3C**). Based on their relative abundance by organ (**Figure 2B**) and expression of surface markers (**Figure 2C**), we identified marrow (NeuP) and splenic (SNeuP) neutrophil progenitors, marrow immNEU (Neu1) and matNEU (Neu2), splenic (SNeu) and circulating (Neu3) neutrophils. Subpopulations with a lower abundance (< 3% of all metaclusters) were not annotated. When focusing on clusters emerging in the spleen during EMH, we found that these subpopulations appeared in the circulation during stress-induced granulopoiesis while not changing in the bone marrow compartment, suggesting a splenic origin (**Figure 2D**). To validate these results, we studied the dynamics of neutrophil differentiation and mobilization to the circulation using 5' bromo-deoxy-uridine (BrdU) pulse-chase experiments (**Figure 2E**). Mice were injected with BrdU 3 days before sacrifice, time required for the BrdU signal to label dividing neutrophil progenitors and to reach the post-mitotic pool (immature and mature neutrophils) before being released to the circulation. We then evaluated the BrdU signal across granulopoiesis as defined by PHATE trajectory ***(11)*** at Zeitgeber time (ZT) 13, *i.e.* the time of neutrophil release to the circulation ***(12)***, and at ZT2 (day time) (**Figure 2E**). Interestingly, $BrdU^+$ neutrophils were found to progress with time within the bone marrow from an immature ($PHATE^{low}$) to a mature ($PHATE^{high}$) state while remaining immature in the spleen. We then binned cells across PHATE dimension 1 into 8 equal-sized clusters (**Figure 2F)**. These clusters defined cells with progressive maturation levels (from bin 1 to 8) as demonstrated by CXCR2 expression (**Figure**

2G). Analysis of these binned clusters on $BrdU^+$ neutrophils showed an absent increase in bin 8 within the spleen thus supporting the inability of immature splenic neutrophils to mature (**Figure 2H, Extended Figure 3D**). These results suggested the possibility that splenic neutrophils are prematurely released to the circulation at an immature state constituting approximately 5-10% of the total of circulating neutrophils in mice treated with CPM/AMD, fed high-fat diet, or repeatedly injected with LPS (**Extended Figure 3E-G**). Furthermore, these results also suggest the disconnection between splenic immature neutrophils and their mature counterparts. Indeed, Pearson correlation analysis of mature and immature neutrophils shows a strong correlation in the bone marrow (**Extended Figure 3H**), but not in the splenic niche (**Extended Figure 3I**). These results therefore indicate that mature neutrophils in the spleen are likely recruited from the circulation rather than being produced *in situ*. Consistently, we found in additional BrdU pulse-chase experiments that while immature neutrophils progressively acquired the signal, mature neutrophils positive for BrdU appeared in the spleen only at the time of their peak in the blood (**Extended Figure 3J**). Altogether, splenic neutrophils constitute a mixture of *de novo*-produced immature neutrophils and mature blood-borne neutrophils.

In line with the concept of a splenic origin of immature neutrophils in the blood, this subpopulation scored higher in our scRNA-seq data for a transcriptomic signature of splenic immature neutrophils as compared to bone marrow immature neutrophils (**Figure 2I**). In further support of this notion, circulating immature neutrophil counts positively correlated with immature neutrophils in the spleen but not the bone marrow (**Figure 2J**). Moreover, pairwise analysis showed minimal differences between SNeu and immature blood neutrophils (**Extended Figure 4A**). Of note, splenic or blood mature neutrophils showed significant transcriptional differences respective to their immature counterparts. These differences were minimal when comparing splenic mature neutrophils to circulating mature cells (**Extended Figure 4A**), suggesting that mature splenic neutrophils are primarily blood-derived as reported previously (***13, 14***). To causally prove the contribution of the splenic granulopoiesis to the circulating neutrophil pool, we performed splenectomy or partial irradiation shielding the abdomen to protect active splenic granulopoiesis prior or after induction of emergency granulopoiesis, respectively (**Figure 2K**). As predicted, flow cytometry analysis (**Figure 2L**) or scRNA-seq analysis (**Figure 2M**) of circulating neutrophils revealed that splenectomized mice showed a reduced presence of immature neutrophils without impacting on the bone marrow neutrophil composition (**Extended Figure 4B/C**); partial irradiation, on the other hand, led to enrichment of circulating immature neutrophils. To further confirm the origin of the circulating immature neutrophils, we employed a mouse model of neutrophil mosaic tracing. Based on the combination of nuclear and cytoplasmic-restricted fluorescent proteins (***15***), this mouse model labels up to 11 detectable mosaics under the control of the neutrophil-specific promoter Mrp8 thus allowing to identify multiple randomly generated color combinations (**Extended Figure 4D**). We first assessed the similarity of mosaic frequencies between each organ and the circulation using correlation analysis (**Extended Figure 4E**). We found that immature neutrophils in the spleen closely resembled those in blood, whereas immature bone marrow neutrophils diverged substantially from the circulating pool (**Extended Figure 4E**, left panel). In contrast, and consistent with our BrdU pulse-chase experiments (**Extended Fig. 3J**), mature circulating neutrophils showed strong similarity to both bone marrow and splenic mature neutrophils (**Extended Figure 4E**, right panel).To specifically investigate the

clones driving these differences, we next identified mosaics that significantly differed in abundance between bone marrow and spleen and repeated the correlation analysis using only these informative clones (**Extended Figure 4F/G**). Because most mature clones did not pass the filtering criteria, we focused on the immature subpopulations. This refined analysis confirmed that immature splenic neutrophils exhibit markedly higher similarity to circulating immature neutrophils than those originating in the bone marrow (**Extended Figure 4F/G**). Taken together, our mosaic-tracing approach, together with the splenectomy and partial irradiation experiments, provides integrated and compelling evidence that the spleen is the predominant source of circulating immature neutrophils.

With immature neutrophils being released exclusively from the splenic niche, we asked the question if retention mechanisms differ from those in the bone marrow. To this end we compared the contribution of molecules known to be involved in neutrophil retention to retention in the spleen and the bone marrow (**Extended Figure 5**). Blockade of the molecules ICAM1, VCAM1, CD44, CD18, CD49d or CD62L using specific antibodies did not specifically altered the retention of SNeu as compared to the other subpopulations (**Extended Figure 5A**). Hence, we evaluated the importance of the two chemokine axes CXCR4 and CXCR2 in site specific retention (**Extended Figure 5B-E**). To this end, we employed mice with neutrophil-specific genetic deficiency of CXCR4 (*Mrp8*^{CRE}*Cxcr4*$^{fl/fl}$) or CXCR2 (*Ly6g*^{CRE}*Cxcr2*$^{fl/fl}$) as compared to respective controls (*Mrp8*^{CRE} and *Ly6g*^{CRE}). Given absence of CXCR4 and CXCR2, we generated PHATE analysis with a combination of all other available markers to unbiasedly assess cell maturation. After PHATE analysis, cells were binned in 5 groups with equal cell numbers, with Phate_01 being the most mature and Phate_05 the most immature. Based on the proportions of PHATE bins in the blood samples, we defined Phate_01 to Phate_03 as the mobilizing pool of neutrophils (with being Phate_03 being the most immature) (**Extended Figure 5B/C**). Interestingly, organ retention analysis showed that CXCR4 absence did not reduce retention of immature neutrophils in the spleen (**Extended Figure 5D**), while absence of CXCR2 lead to a significant reduction in the spleen as compared to the bone marrow (**Extended Figure 5E**). Furthermore, analysis of CXCR2 and CXCR4 ligands in the splenic niche showed that MPO^{+} cells were in closer proximity to *Cxcl1* transcripts as compared to *Cxcl12* (**Extended Figure 5F-H**). Together, these suggest that CXCR4 elicits bone marrow-specific neutrophil retention, while CXCR2 signaling retains SNeu in the spleen. Thus, lower expression of CXCR2 in SNeu might link to their rapid release to the circulation, a phenomenon aggravated in neutrophils with complete absence of CXCR2 molecule. In summary, splenic granulopoiesis generates neutrophils that prematurely exit their site of production delivering immature neutrophils to the circulating neutrophil pool.

Clustered myeloid progenitors engage in accelerated splenic granulopoiesis

Stress-induced granulopoiesis copes with neutrophil demand by conveying a rapid stem cell division and enhanced cell differentiation towards neutrophils. Mechanistically, under stress conditions, neutrophil differentiation is fast-tracked by shorter differentiation pathways. This is facilitated by clustered myeloid progenitor positioning close to vascular niches (***16***) and enhanced abundance of growth factors such as G-CSF (***1***). We hence speculated that SNeuP engage in a rapid differentiation process preceding the premature release of neutrophils to the circulation thus offering an explanation for the enrichment of an immature stage.

BrdU pulse experiments performed within a 24-hour time window showed a profound dilution of the signal from the preNEU towards the immNEU state within the spleen as compared to the bone marrow (**Figure 3A, Extended Figure 6A**), suggesting an accelerated maturation at the preNEU to immNEU intersect. Furthermore, splenic preNEUs were intrinsically poised for division and differentiation, as isolated preNEUs incubated with growth factors or bone marrow supernatants gave rise to an increased number of descendants (**Extended Figure 6B**). To test the importance of the splenic environment to activate these progenitors, bone marrow-isolated progenitors from dsRED mice (red-fluorescent) were adoptively transferred into the spleen of C57BL6 mice by subcapsular injection (**Figure 3B, Extended Figure 6C**). Eight days after the injection, SNeuP differentiated into neutrophils, and we observed a positive correlation between cKit$^+$ cells and neutrophils in the spleen (**Extended Figure 6C**). Interestingly, dsRED$^+$ neutrophils exhibited a reduced maturation (lower expression of CXCR2) as compared to endogenous neutrophils (**Figure 3B**), suggesting that the spleen environment was sufficient to drive this altered cell differentiation.

Stress-induced myelopoiesis within the bone marrow alters progenitor spatial positioning with enhanced clustering (***16***) and generation of lineage-specific production sites (***17, 18***). Based on these studies, we profiled the spatial distribution of myeloid progenitors within the spleen and bone marrow (**Figure 3C-G**). We assessed the myeloperoxidase (MPO) expression pattern which represented a *bona fide* marker for differentiation from GMP towards mature neutrophils as found with flow cytometry analysis and intracellular staining (**Extended Figure 6D/E**) and immunofluorescence on sorted cells (**Extended Figure 6F**). EMH in the spleen was visible as isolated clusters within the red pulp, a structure not found in homeostasis (**Figure 3C, Extended Figure 7A/B**). Interestingly, neutrophils with an immature phenotype (dispersed MPO signal and reduced Ly6G expression, cluster 3) were situated close to their progenitors but distant to mature cells as compared to randomly distributed cells (**Figure 3D**), demonstrating the formation of neutrophil production sites around clustered myeloid progenitors. Splenic clusters were enriched in immature neutrophils and progenitors with reduced numbers of mature neutrophils as compared to clusters formed in the bone marrow niche (**Extended Figure 7C**). Furthermore, distance analysis between mature and immature neutrophils showed an increased spacing in the spleen as compared to bone marrow under control or CPM/AMD treatment (**Figure 3E**), thus confirming the disconnection between resident mature splenic neutrophils and the immature counterparts. To extend these analyses to human biology, we analyzed the proportion of myeloid progenitors in the human spleen by flow cytometry (**Extended Figure 8A**). Here, GMPs were present in the human spleen in a similar proportion as compared to human bone marrow and higher than in cord blood. Interestingly, human splenic GMPs differentiated preferentially into neutrophil-like cells as compared to monocytes (**Extended Figure 8B**), supporting the neutrophilic bias of splenic myeloid progenitors found in mice (**Extended Figure 2C**). To investigate the spatial distribution of myeloid progenitors and their descendants, we performed multiplexed imaging on spleens obtained from human organ donors (**Figure 3F/G, Extended Figure 8C-E**). Using histocytometry, we clustered neutrophilic cells (CD11b$^+$CD15$^+$) into 5 maturation stages based on the expression of MPO and CD117 (**Figure 3G**, **Extended Figure 8C-E**). This analysis corroborated the enrichment with cells with an immature phenotype (**Extended Figure 8E**). We then used a Ripley's K-function

to assess whether the identified cells were clustered or randomly distributed (**Figure 3G**). Here, clusters with a progenitor ($MPO^{high}CD117^{high}$) or immature phenotype ($MPO^{high}CD117^{high/med}$, $MPO^{high}CD117^{med}$) displayed values that deviated from a homogenous Poisson distribution (Theoretical Poisson) supporting their clustered distribution (**Figure 3G**). Interestingly, these cell clusters are located in the red pulp (**Figure 3F**) and in close proximity to vessels (**Extended Figure 8C**).

Epigenetic rewiring drives splenic neutrophil differentiation routes

To understand splenic differentiation dynamics, we performed trajectory inference analysis on our scRNA-seq. PAGA analysis revealed a main production and differentiation trajectory (Milestone 9 to 10, **Figure 4A** and **Extended Figure 9A-C**) but also a pronounced accumulation at early stages of the trajectory (**Figure 4B**) defined by a second path (Milestone 3, **Figure 4A**). Velocity analysis confirmed this differentiation pathway that deviated from the bone marrow main route (**Figure 4C/D**). Next, we questioned whether splenic neutrophils with an immature profile constituted an end-stage cell within the differentiation pathway. We hence sorted cells at the immature stage, and adoptively transferred them into a mouse under steady-state condition (**Figure 4E**). 16 hours after transfer, we assessed the expression of markers of maturation such as CD101 and CXCR2 (**Figure 4E**, **Extended Figure 9D**). Interestingly, we found that immature neutrophils originating from the bone marrow acquired expression of these markers, while splenic immature neutrophils failed to acquire maturation markers. In agreement with this intrinsic inability to adopt a mature phenotype, *in vitro* assessment of differentiation of immature neutrophils from bone marrow and spleen showed that spleen-derived cells had a reduced ability to fully mature of spleen-derived cells (**Extended Figure 9E**). Thus, these results culminate in a concept that neutrophils produced in the spleen rapidly differentiate into an end-stage immature subpopulation that constitutes the end of their maturation path.

To obtain further insight into the mechanisms driving this accelerated differentiation, we profiled the epigenetic changes occurring at the stage of the neutrophil progenitor. We performed ATAC-seq (Assay for transposase-accessible chromatin followed by sequencing) in sorted GMPs, preNEU, immNEU and matNEU from the bone marrow, spleen, and blood (**Figure 4F/G, Extended Figure 9F-H**). Principal Component Analysis (PCA) showed that samples primarily clustered based on cell type (**Extended Figure 9F**). Subsequent unbiased clustering resulted in 5 main clusters of open chromatin regions (**Figure 4F/G**). Enrichment score analysis on these 5 clusters revealed an increased presence of motifs for CEBP transcription factor (TF) family (CEBPα, CEBPβ, CEBPδ, CEBPε, CEBPγ) and RUNX1 and RUNX2 in cluster 1 (C1) which is associated with neutrophil maturation (**Figure 4F**) (***19***). Peaks of cluster 3 (C3) were enriched in motifs for Interferon Regulatory Factor (IRF, IRF1, 4 and 8) and STAT families, PU1 motifs for cluster 4 (C4) and AP-1 family motifs for cluster 5 (C5, JunD, JunB, Fos). As found by scRNA-seq, the chromatin accessibility of the maturation cluster C1 reflected the similarity between mature cells in the spleen and blood, suggesting their similar origin, and their striking difference with the immature splenic cells (**Figure 4G**). At the progenitor level, paired evaluation of general open peaks analysis showed an increased number of differential open chromatin regions in splenic GMPs, suggesting an active status at this level of development (**Extended Figure 9G**). These open peaks were particularly enriched in C1 cluster, supporting an active differentiation phenotype

(**Extended Figure 9H**). Of note, while no differences were found in the expression of the receptor for G-CSF, splenic GMPs showed increased levels of GM-CSF and IL-3 receptors previously associated with proliferative progenitors in emergency granulopoiesis (**Extended Figure 9I**) (***20, 21***). To further investigate the differentiation dynamics of SNeus, we unbiasedly identified patterns of gene expression along differentiation and maturation by assessing their epigenetic profiles across bone marrow and spleen (**Extended Figure 10**). We employed a dataset from Evrard et al (***22***) where bulk RNA-seq was performed on bone marrow GMPs, preNEU, immature and mature neutrophils and circulating mature neutrophils at ZT5 and ZT13. Using linear regression analysis, we identified 4 clusters (**Extended Figure 10A**) characterized by the different expression profiles along the differentiation path (**Extended Figure 10B**). Of note, Cluster 1 and 2 vs. Cluster 3 and 4 showed similar profiles with increasing or decreasing expression along differentiation, respectively. Using these signatures, we first profiled in our ATAC-seq data differentially opened and closed peaks within 30kb upstream and downstream of genes of these four clusters (**Extended Figure 10C/D**). The number of open and closed peaks (spleen vs bone marrow) showed an overall open chromatin landscape at the level of the splenic GMP that was reduced in the subsequent cell states (preNEU and immNEU) (**Extended Figure 10C**). Detailed analysis of the 4 clusters showed that, in the spleen, Cluster 1 (increasing gene expression from GMP to mature neutrophils) exhibited more open peaks at the GMP stage and closed at the preNEU and immature neutrophil level (**Extended Figure 10D**) constituting the main cluster of genes that defined the overall chromatin differences between spleen and bone marrow. The other 3 clusters remained open in the spleen at each cell stage as compared to the bone marrow. Next, we assessed whether those altered chromatin peaks related to changes at RNA level. Since in our scRNA data set the number of GMPs was limited, we performed a bulk RNA-seq on GMPs from the bone marrow and the spleen of mice treated with CPM/AMD (**Extended Figure 10E**). In this dataset, we assessed the expression of each cluster confirming that Cluster 1 and 2 genes were generally more expressed in splenic GMPs as compared to their bone marrow counterparts (**Extended Figure 10E**). To define the dynamics of these clusters from neutrophil progenitors towards neutrophils, we then focused on our scRNA-seq data (**Extended Figure 10F**). We calculated and plotted the signature score across the pseudotime values (as an approximation of maturation) and focused on the trendline calculated from origin to the release to the circulation (spleen until 0.15 pseudotime value indicated by dashed line, and bone marrow until 0.25). Interestingly, levels of RNA transcripts were similar or higher in the spleen for each cluster as compared to bone marrow (**Extended Figure 10F**). These data indicate that the fast differentiation occurring in the spleen causes rapid gene transcription and chromatin closure (in line with our BrdU pulse-chase experiments, **Figure 3A**). We next focused on specific maturation markers such as CXCR2 or CD101, which are lower expressed at protein level in SNeu. Here, analysis of the chromatin landscape showed a closed chromatin signature for *Cxcr2* but not for *Cd101* (**Figure 4H/I**) that was also identified at RNA level suggesting an impaired expression of *Cxcr2* (**Figure 4J**). Interestingly, *Cd101* expression in the bone marrow only ramped up at the end of the maturation, i.e. after the point of release of splenic neutrophils (dashed line, **Figure 4J**). These results indicate that the rapid mobilization of these cells might impede the transcriptional upregulation of *Cd101*, thereby explaining the lack of expression of this marker in circulating splenic neutrophils. We conclude from these results that the splenic microenvironment

provides a platform for the rapid differentiation of neutrophil progenitors towards SNeu reflected by accelerated transcription of maturation genes paralleled by an increased chromatin inaccessibility.

Splenic neutrophils propel host defense through interferon priming

We next sought to assess the functionality of spleen-derived neutrophils by profiling relevant neutrophil antimicrobial effector functions such as reactive oxygen species (ROS) production or Neutrophil Extracellular Trap (NET) formation. At transcriptomic level, splenic immature neutrophils showed enrichment in genes associated with NETosis, neutrophil activation, and ROS production (**Figure 5A, Extended Figure 11A/B)**. Furthermore, splenic neutrophils are characterized by increased expression of genes related to anti-bacterial or anti-fungal response. Our functional analysis confirmed these transcriptomic differences showing an increased ROS production (**Figure 5B, Extended Figure 12A**) in SNeu as compared to mature Neu3 neutrophils within the blood compartment. Similary, SNeu from the spleen also exhibited increased intracellular (**Extended Figure 12B, 12C**) and extracellular (**Extended Figure 12D**) ROS production. In line with the increased ROS production, NETosis in response to LPS was augmented in circulating immature as compared mature neutrophils (**Figure 5C**). Finally, analysis of bacteria killing demonstrated that SNeu exhibited an increased microbicidal capacity as compared to their bone marrow counterparts (**Extended Figure 12E**). Of note, phenotypic analysis of FACS-sorted neutrophils showed that circulating immature neutrophils exhibited elevated expression of MPO and CD11b as compared to mature neutrophils (**Extended Figure 12F**). As expected, sorted neutrophils showed a prototypical nuclear band-shape for immature neutrophils irrespective of the organ of origin (**Extended Figure 12F**). On the other hand, granule protein content exemplified by myeloperoxidase (MPO, primary granules) or CD11b (tertiary granules) as well as cytoplasmic S100A8 showed no differences between bone marrow and splenic neutrophils. Contrary to observations made by others where immature neutrophils exhibit reduced effector capacity (***23***), we here show that SNeu produced during hematopoietic stress display similar or greater antimicrobial effector functions compared to neutrophils originating from the bone marrow despite their immature phenotype. We hence tested the antimicrobial abilities of SNeu in a model of UPEC-induced bladder infection (**Figure 5D, Extended Figure 13A**). Here, we analyzed the number of bacterial colonies in the bladder of CPM/AMD-treated mice in absence of the spleen and after adoptive transfer of splenic or bone marrow neutrophils. In line with their enhanced effector properties, lack of splenic neutrophils in splenectomized mice increased bacterial burden, an effect fully reverted by adoptive transfer of splenic neutrophils (**Extended Figure 13A**, **Figure 5E**). No changes were found in neutrophil numbers within the circulation or bladder tissue (**Extended Figure 13B-F**). The augmented antimicrobial capability of SNeu was also corroborated after adoptive transfer of FACS-sorted neutrophil subpopulations isolated from bone marrow and spleen into splenectomized mice (**Extended Figure 13G-J**). Altogether, we demonstrate that SNeu are endowed with an enhanced antimicrobial potency and help containing bacterial growth under host infection.

We next sought to understand the molecular mechanism underlying the antimicrobial characteristics of spleen-derived immature neutrophils. From our chromatin analysis, we unbiasedly identified an increased enrichment of IRF and STAT transcription factor families in cluster (C3, **Figure 4F/G**), whose open peaks were particularly

increased in SNeuP (**Figure 6A**). This permissive chromatin state correlated with an increased type I interferon and STAT signaling at RNA level within this cell subpopulation (**Figure 6B**). Importantly, this increased type I interferon at the progenitor level was confirmed in other models such as in hypercholesterolemia (**Extended Figure 14A**) and melanoma (**Extended Figure 14B**), excluding a model-dependent result. Furthermore, SNeuP showed reduced TGFβ signaling, which is in accordance with an enhanced progenitor differentiation and reduced regeneration and entrance into quiescence (15). We then hypothesized that the elevated interferon signaling at the progenitor level might confer these enhanced antibacterial responses as previously proposed in the context of trained immunity (***24, 25***). Furthermore, we speculated that this interferon priming was restricted to the spleen environment as was previously shown for dendritic cells (***26***). In agreement with this idea, the levels of IFNβ (**Figure 6C**) and the proportion of progenitors expressing high levels of the interferon-responsive protein IFIT1 is enhanced in the spleen as compared to the bone marrow (**Figure 6D/E**). To causally test the importance of interferon signaling, we employed a mouse model lacking Interferon-alpha/beta receptor signaling in neutrophils (*Mrp8*^{cre}*Ifnar1*$^{fl/fl}$). *Mrp8*^{cre}*Ifnar1*$^{fl/fl}$ and *Mrp8*^{wt}*Ifnar1*$^{fl/fl}$ were subjected to splenectomy or sham treatment, followed by CPM/AMD application prior to bacterial infection (**Figure 6F**). Importantly, deletion of Type I interferon signaling in neutrophils did not affect the number of circulating neutrophils with an immature phenotype which were dramatically reduced after splenectomy (**Figure 6G**). On the other hand, analysis of surface marker expression in circulating neutrophils showed no differences in neutrophil activation before infection but a marked reduction in activated neutrophils upon bacteria administration (Cluster 3, **Figure 6H-J**). No changes in the absolute number of circulating mature neutrophils, total neutrophils, or monocytes before (**Extended Figure 14C-E**) or circulating immature neutrophils, mature neutrophils, or monocytes after infection (**Extended Figure 14F-H**) were detected between the two genotypes. Similarly, no differences were found in tissue-infiltrated neutrophils within the bladder (**Extended Figure 14I-L**). Confirming our previous, results splenectomy gave rise to a defective containment of the bacteria. Mice lacking Type I interferon signaling in neutrophils had an impaired ability to contain and clear bacteria (**Extended Figure 14M**), an effect not further accentuated when removing the spleen (**Figure 6L**). Collectively, these results demonstrate a role of the spleen environment for the priming of neutrophils produced in the spleen. Specifically, our data point towards the importance of Type I interferon signaling to maintain host defense fitness during stress-induced granulopoiesis.

Discussion

Host immune responses against long-lasting stressors are associated with a profound remodeling of the hematopoietic compartment that is biased towards myeloid differentiation. Granulopoiesis is particularly prioritized under multiple continuous sterile and infectious challenges and constitutes an important use of energy that challenges the capacity of the bone marrow (***1***). Under certain inflammatory scenarios, granulopoiesis can be re-routed to other tissues that host hematopoietic progenitors that generate neutrophils; these potentially support the bone marrow production and maintain the immune response. Although generally considered a side-effect of persistent inflammation, the role of extramedullary neutrophil production and its contribution to host defense is understudied. Here, we identify an alternative yet accelerated neutrophil production in the spleen generating

terminally differentiated cells with enhanced antimicrobial capacity contributing to pathogen containment. First, mapping stress-induced splenic granulopoiesis across a variety of perturbations characterized by low chronic inflammation revealed a generalized bias towards the generation of neutrophils with an immature phenotype. Second, splenic neutrophil progenitors are activated to rapidly differentiate into neutrophils that continuously exit their niche, feeding the circulating pool. Third, type I interferon priming of splenic progenitors links to production of neutrophils with enhanced effector function.

Persistent inflammation in unresolved infections initiates an evolutionarily conserved program of emergency granulopoiesis to cope with the need for neutrophils required to fight invading pathogens (***27***). Features of this programmed response are conserved across a variety of persistent low-grade inflammatory conditions, including cardiometabolic stress, cancer, and chronic infection (***20, 22, 28-33***). Among these features, the elevated production of immature neutrophils and their premature release to the circulation is a hallmark of these pathologies and is commonly associated with disease severity (***34-39***). In addition to confirming the mild expansion of neutrophil progenitors and immature neutrophils within the bone marrow, we here identify a strikingly increased granulopoiesis within the spleen peaking at the stages of preNEU and immature neutrophils. The similar proportion of these subpopulations within the bone marrow also suggests that both granulopoiesis pipelines are governed by common differentiation hierarchies primarily arising at the level of the preNEU as previously suggested (***22***). However, the rate of cell differentiation differs significantly between the two niches, with splenic neutrophil progenitors outperforming the capacity of their bone marrow counterparts. Our trajectory and epigenomic analysis also show that this heightened progenitor activity is accompanied by a more rapid differentiation route to generate and release effector neutrophils in a shorter time frame. Notably, this prompt mobilization relies on distinct chemotactic axes: the CXCL12-CXCR4 pathway regulates bone-marrow retention and egress, whereas the CXCL1-CXCR2 axis predominantly governs splenic neutrophil mobilization. This division of labor ensures that each hematopoietic organ adjusts neutrophil output according to host requirements. These two processes (cell differentiation and mobilization) might have evolved in parallel within the spleen environment to efficiently cope with neutrophil demands and to accelerate the elimination of the invading pathogens. On the other hand, the activation of this program under chronic sterile inflammatory perturbations is probably associated with the previously observed pathogenic contribution of spleen-derived myeloid cells in mice (***5, 7, 20, 40***) and humans (***41, 42***). Moreover, our study also reveals the disparate origins of splenic neutrophils. The disruption in cell maturation during splenic granulopoiesis with immediate exit to the bloodstream indicates that the identified mature neutrophil population in the spleen is not produced on site. Our data demonstrate a phenotypic, spatial, and functional separation between immature and mature splenic subsets in both mouse models and in human spleen specimens. Therefore, we propose that this mature splenic population is in fact blood-borne, and probably contributes to the local function of these subpopulations or the clearance of circulating aged neutrophils. Consequently, future functional studies on neutrophils produced during EMH should carefully discriminate between discrete subsets when comparing neutrophils of different maturation states and origin.

Our observations support a stress-driven granulopoiesis even under situations of low chronic inflammation. While the existence of the immature neutrophils in the circulation ("left-shift") is commonly associated with an increase of discharge-inducing signals that surpass the signaling threshold necessary for inducing neutrophil mobilization to the blood, their appearance under chronic stress cannot be explained by a compensatory mechanism to meet the demand of cells. In fact, the release of these cells might be a consequence of (1) a collateral effect of a dysfunctional granulopoiesis or (2) an active process to deal with the instigating stimulus. For the first possibility, our transcriptomic and epigenetic data shows that splenic GMPs have an increased number of open chromatin peaks at cluster 1, which is enriched for TFs involved in differentiation and maturation as compared to those found in the bone marrow, supporting an activated and differentiative phenotype as previously suggested **(*43*)**. This rapid differentiation is accompanied by a heightened transcription rate and progressive chromatin compaction. Hence, this epigenetic and transcriptional status explains the observed elevated proliferation and differentiation capacity and might consequently result in the generation of neutrophils with reduced maturation. Interestingly, the premature release of splenic neutrophils might precede the expression of late maturation markers such as *Cd101*, thus explaining their reduced levels and incomplete maturation phenotype. Furthermore - and despite stem cells and progenitors exhibiting similar levels of G-CSF receptor in both organs -, HSPCs of splenic origin displayed increased levels of IL-3 and GM-CSF receptors. This may elevate their responses to growth factors involved in stem cell survival and proliferation during emergency hematopoiesis **(*20, 21*)** and thus support an enhanced intrinsic splenic neutrophil progenitor responsiveness and activity. Our spatial analysis also revealed that splenic neutrophils originate from clustered production sites in the red pulp, an active process that is part of the emergency granulopoiesis program, as previously suggested **(*16*)**. Notably, this clustered production of neutrophils within the red pulp can also be inferred from our analyses of human spleen samples obtained from organ donors, suggesting that this process is conserved across species. However, the functional consequences of this process in human infectious diseases, cancer, or metabolic pathologies remains to be studied.

On a functional level, our results illustrate an alternative differentiation pathway in the spleen to rapidly generate fully competent neutrophils. In contrast to their immature phenotype, spleen-derived neutrophils are fully armed with antimicrobial effector functions that help to contain and eliminate invading bacteria. Contrasting data showing reduced **(*44*)**, similar **(*45*)** or increased **(*46, 47*)** functional properties of phenotypically immature neutrophils suggest that the function of these cells may be context- and origin- dependent. Using adoptive transfer strategies, we here provide causal evidence for the beneficial role of spleen-borne immature neutrophils in the context of infections, yet genetic tools to modulate the levels and functions of this subpopulation are necessary to dissect their role in greater depth. Importantly, the pathogen-containing properties of spleen-derived immature neutrophils are in agreement with the concept of an active, on-demand production of this subpopulation in response to inflammatory stress. Mechanistically, we demonstrate that the spleen can host the production of these neutrophils due to its niche characteristics and the ability of progenitor priming through type I interferons. Given the functionality of these cells, it is plausible that the selective mobilization of neutrophils at different stages of maturation might help adapt the host neutrophil

circulating pool to specific inflammatory responses depending on the functional needs. Such concept is exemplified by the program of “neutrophil aging”, which generates cell subpopulations that meet different functions across the day and in synchrony with the higher likelihood of exposure to external challenges during the activity phase (***48, 49***). This functional plasticity can also be achieved by releasing neutrophils with various degrees of maturation exhibiting distinct epigenetic and metabolic properties, allowing them to adapt to different environments counterparts (***46***), or to strongly react to invading pathogens under life-threatening conditions.

The coexistence of mature and immature neutrophil subsets in altering proportions under different pathological conditions may lead to different disease outcomes and is likely to be disease-dependent. On the other hand, in non-infectious diseases, the existence of this subpopulation could cause undesired effects due to its persistent action in the absence of an invading pathogen. However, this possibility remains to be investigated in future studies. In conclusion, we show that the spleen serves as an immune-supporting platform to produce neutrophils with enhanced antimicrobial function to cope with infections under prolonged stress. Our findings illustrate a host mechanism that exploits increased neutrophil plasticity and cell maturation as a source of functional heterogeneity to generate rapid and effective responses against invading pathogens.

Acknowledgements

We thank Ulrich Dobrindt (University of Münster) for providing the uropathogenic *E.coli* strain used for the infection experiments. This project was supported by the Else Kröner Fresenius Stiftung (2017_A13) and the Deutsche Forschungsgemeinschaft (CRC TRR332 project A1). C.S.R. receives support from IZKF of University of Münster. O.S. receives support from the Deutsche Forschungsgemeinschaft (CRC TRR332 projects A2 and Z1, CRC1123 project A6, CRU342 project 1, project 502158695, SO876/16-1), the Leducq Foundation, Novo Nordisk, the EU (PRAETORIAN Doctoral Network), the Else Kröner Fresenius Stiftung (2023_EKSE.212), and the IZKF and the IMF of the University of Münster. D.R.E. is supported by the Deutsche Forschungsgemeinschaft (CRC TRR332 project A3). J.J. is supported by the Deutsche Forschungsgemeinschaft (CRC TRR332 project A5). T.C. is supported by the Deutsche Forschungsgemeinschaft (CRC TRR332 project B4). M.P.-S was supported by grants from the Spanish Ministerio de Ciencia, Innovación y Universidades (MICIN) (RYC2021-033511-I and PID2022-141878OA-I00). E.O. was supported by a grant from Junta de Extremadura-Fondo Europeo de Desarrollo Regional (GR24071). F.A.C is supported by a predoctoral fellowship from the Spanish MICIN (PREP2022-000398). –This study was partially supported by the Münster Imaging Network - Preclinical Imaging (RI_00497).

Author contributions

C.S.R., R.C., and O.S., conceptualized the study and designed experiments. C.S.R., performed most of the experiments and analyzed data. R.C., M.F., A.B., V.S., M.R. and M.P.-S. performed experiments and analyzed data. L.M.V., A.H., **F.A.C.**, Q.B., M.G., J.S., S.S., P.L., C.T., Y.B., A.H.C., H.F., S.R.G., C.O.S., performed experiments. M.R., helped with MACsima image acquisition and analysis. D.A., C.M., helped with mass cytometry (CyTOF) panel design and generation, and data acquisition. A.B. and F.R., performed, analyzed and helped for interpretation of

ATAC-seq data. R.Z., helped with bulk RNA analysis. N.A.G., provided cell sorting platform. E.O., provided support for neutrophil mosaic experiments. S.L., and U.K., provided reporter mouse model of Interferon beta luciferase. Y.B., and S.L., helped with infection analyses. D.R.E., helped with intraurethral infection model. M.G., J.S., A.C., designed, performed and acquired data of flow cytometry analysis of human spleen and in vitro differentiation of splenic progenitors. A.K., provided human spleen specimens for imaging. R.B., A.H., M.P.-S and F.A.C provided the mouse model and performed experiments for the neutrophil mosaic analysis. J.J., provided scRNA-seq dataset for murine oropharyngeal carcinoma. C.S.R., and O.S., wrote the manuscript. R.C., A.B., M.R., P.D., A.H., T.C., edited and provided comments to the manuscript. C.S.R., and O.S., funded the project.

Declaration of interest

The authors declare no conflict of interest.

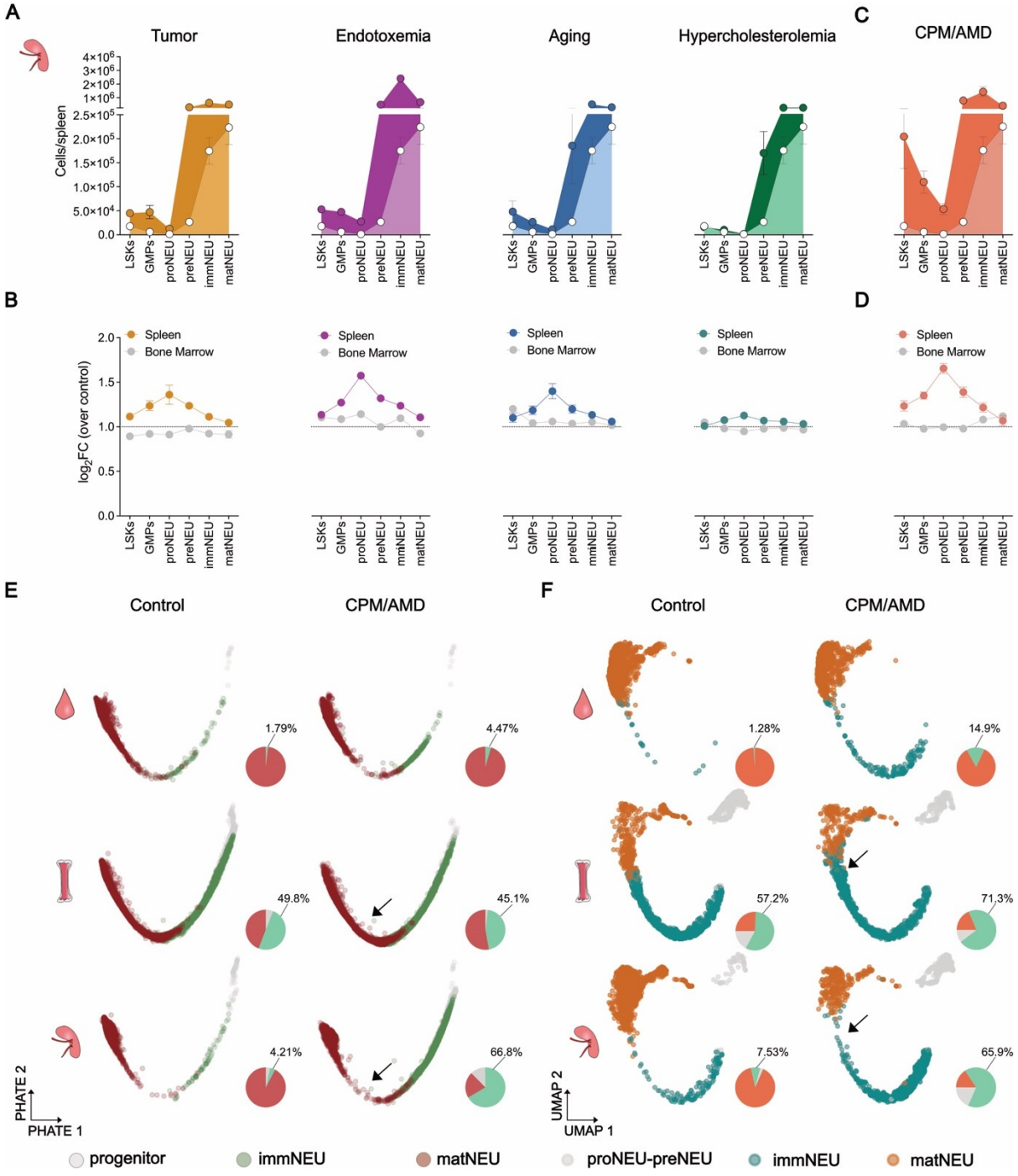

Figure 1. **Alternative neutrophil production dynamics in stress-induced splenic granulopoiesis. (A/B)** Flow cytometry-based quantification of indicated stages of granulopoiesis in the spleen. LSKs ($Lin^-Sca1^+cKit^+$), granulocyte-macrophage progenitors (GMP, $Lin^-Sca1^-cKit^+CD16/32^{high}CD34^+$), neutrophil-specified (proNEUs, $Lin^-Sca1^-cKit^+$ $CD16/32^{high}Ly6C^+CD115^-CD81^+CD11b^+$) and -committed progenitors (preNEU, $Lin^-cKit^{int}Ly6C^+CD115^-CD11b^+CXCR4^+$), immature (immNEU, $CD11b^+Ly6G^+CD115^-CXCR2^-$) and mature neutrophils (matNEU, $CD11b^+Ly6G^+CD115^-CXCR2^+$). Data points indicate the mean of 3-10 mice. Lin: Lineage. 8-12 weeks old female C57BL6/J mice with the exception of ageing model. From left to right: tumor model of melanoma, chronic endotoxemia, aging, hypercholesterolemia. (A) Empty circles indicate respective splenic cell populations

under steady-state (control) condition. Filled circles represent counts for each maturation stage in each model. (B) Log2 fold change of each indicated stages over respective control in bone marrow or spleen granulopoiesis. **(C/D)** C57BL6/J female mice (8-12 weeks old) were administered with cyclophosphamide (CPM), followed by daily administration of 5 mg/kg of AMD3100 (AMD). Flow cytometry-based enumeration (C) and log2 fold change over respective control (D) of stages of granulopoiesis in bone marrow and spleen. **(E)** PHATE analysis (calculated from expression of CD101, CD14, CD24, LY6G, CD11b, CD49d, cKIT, CD62L, CD44, CXCR4, CCR2, CXCR2, CD80, CD16) of flow cytometry data on neutrophils and their progenitors from control or CPM/AMD-treated mice of indicated organs. Pie charts depict the proportion of neutrophil progenitors, immature (immNEU) and mature (matNEU) neutrophils. Percentage for immNEU is indicated. n = 5 mice. **(F)** Uniform manifold approximation and projection (UMAP) plot of aggregated cells from scRNA-seq analysis of blood, bone marrow and spleen neutrophil progenitors and descendants colored by cell type. Pie charts depict the proportion of neutrophil progenitors (proNEU_preNEU), immature (immNEU) and mature (matNEU). Percentage for immNEU is displayed. n = 4 mice. Arrows point at continuous vs disrupted granulopoiesis in bone marrow or spleen, respectively.

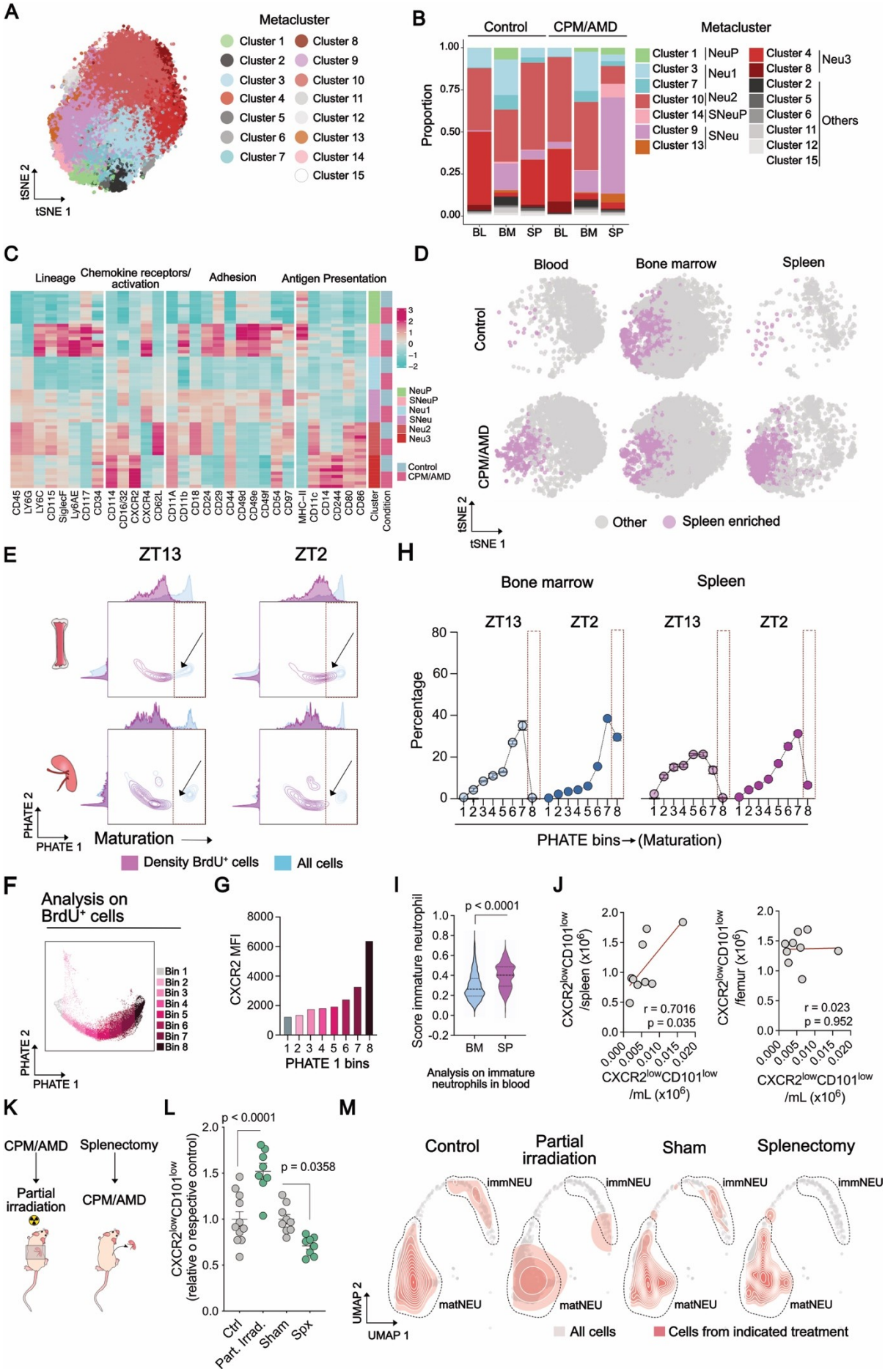
A
Metacluster
Cluster 1
Cluster 2
Cluster 3
Cluster 4
Cluster 5
Cluster 6
Cluster 7
Cluster 8
Cluster 9
Cluster 10
Cluster 11
Cluster 12
Cluster 13
Cluster 14
Cluster 15
tSNE 2
tSNE 1
B
Control
CPM/AMD
Metacluster
Proportion
BL
BM
SP
NeuP
Neu1
Neu2
SNeuP
SNeu
Neu3
Others
C
Lineage
Chemokine receptors/ activation
Adhesion
Antigen Presentation
CD45
LY6G
LY6C
CD115
SiglecF
Ly6AE
CD117
CD34
CD114
CD16/32
CXCR2
CXCR4
CD62L
CD11A
CD11b
CD18
CD24
CD29
CD44
CD49d
CD49e
CD49f
CD54
CD97
MHC–II
CD11c
CD14
CD244
CD80
CD86
Cluster
Condition
NeuP
SNeuP
Neu1
SNeu
Neu2
Neu3
Control
CPM/AMD
D
Blood
Bone marrow
Spleen
Control
CPM/AMD
tSNE 2
tSNE 1
Other
Spleen enriched
E
ZT13
ZT2
PHATE 2
PHATE 1
Maturation
Density BrdU⁺ cells
All cells
H
Bone marrow
Spleen
ZT13
ZT2
Percentage
PHATE bins→(Maturation)
F
Analysis on BrdU⁺ cells
Bin 1
Bin 2
Bin 3
Bin 4
Bin 5
Bin 6
Bin 7
Bin 8
PHATE 2
PHATE 1
G
CXCR2 MFI
PHATE 1 bins
I
p < 0.0001
Score immature neutrophil
BM
SP
Analysis on immature neutrophils in blood
J
CXCR2lowCD101low /spleen (x10⁶)
r = 0.7016
p = 0.035
CXCR2lowCD101low /mL (x10⁶)
CXCR2lowCD101low /femur (x10⁶)
r = 0.023
p = 0.952
CXCR2lowCD101low /mL (x10⁶)
K
CPM/AMD
Splenectomy
Partial irradiation
CPM/AMD
L
p < 0.0001
p = 0.0358
CXCR2lowCD101low (relative o respective control)
Ctrl
Part. Irrad.
Sham
Spx
M
Control
Partial irradiation
Sham
Splenectomy
immNEU
matNEU
UMAP 2
UMAP 1
All cells
Cells from indicated treatment

Figure 2. Premature release of splenic immature neutrophils contributes to the blood neutrophil pool. C57BL6/J female mice were administered with cyclophosphamide (CPM), followed by daily administration of 5 mg/kg of AMD3100 (AMD). **(A-D)** Mass cytometry analysis of blood, bone marrow and spleen neutrophils in steady state or after CPM/AMD treatment. n=5 mice/condition. **(A)** tSNE plot of aggregated cells from blood, bone marrow and spleen neutrophil progenitors and descendants colored by metacluster. (**B**) Proportion analysis of enriched subpopulations within blood, bone marrow and spleen under Vehicle (Control) or CPM/AMD-treatment. BL: Blood; BM: Bone marrow; SP: Spleen. (**C**) Heatmap showing scaled expression of surface receptors within each enriched subpopulation, grouped by function. (**D**) tSNE plot showing spleen-enriched population (magenta) over all cells (light gray). **(E-H)** Mice receiving CPM/AMD were injected 5´Bromo-deoxyuridine (BrdU) 3 days before sacrifice at Zeitgeber Time (ZT)13 or ZT2. **(E)** Plots showing PHATE analysis (markers used: SSC, FSC, AF, CXCR2, LY6G, CD34, CD11b, CD49d, CD16/32, Sca1, CD115, cKIT, CD106, CXCR4, Ly6C and CD81) in indicated organs and time points. Blue and magenta density depicts all and $BrdU^+$ lineage negative cells (Lin: $B220^+CD19^+CD90.2^+CD3^+NK1.1^+F4/80^+$ $FcR\varepsilon^+TER119^+$), respectively. Dashed line indicates the disruption in maturation, while the arrow points at the progression of maturation in the bone marrow. **(F)** Binning of PHATE1 dimension. **(G)** CXCR2 expression across PHATE1 bins. **(H)** Percentage of PHATE1 bins within $BrdU^+$ neutrophils for indicated organs in CPM/AMD-treated mice. Dots indicate mean of 5 mice. **(I)** Enrichment analysis of bone marrow or spleen immature signatures obtained from scRNA dataset assessed in circulating immature neutrophils. **(J)** Pearson correlation of immature ($Ly6G^+CD101^{low}CXCR2^{low}$) neutrophils in bone marrow vs blood (left panel) and spleen vs blood (right panel). Every dot represents one mouse. **(K-M)** Mice under CPM/AMD were subjected to splenectomy or partial irradiation shielding the spleen. **(K)** Scheme of experimental procedure. **(L)** Quantification of immature neutrophils ($Ly6G^+CD101^{low}CXCR2^{low}$) in blood. Data are mean±SEM, two-sided t-test analysis relative to the mean of the respective control. **(M)** scRNA-seq analysis of circulating neutrophils from mice subjected to splenectomy or sham followed by CPM/AMD treatment or mice subjected to CPM/AMD treatment followed by partial irradiation with 6.5 Gy combined with lead radiation shielding of the abdominal area. UMAP plot showing aggregated cells from all treatments (grey) and overlayed density of cells from indicated treatment (red).

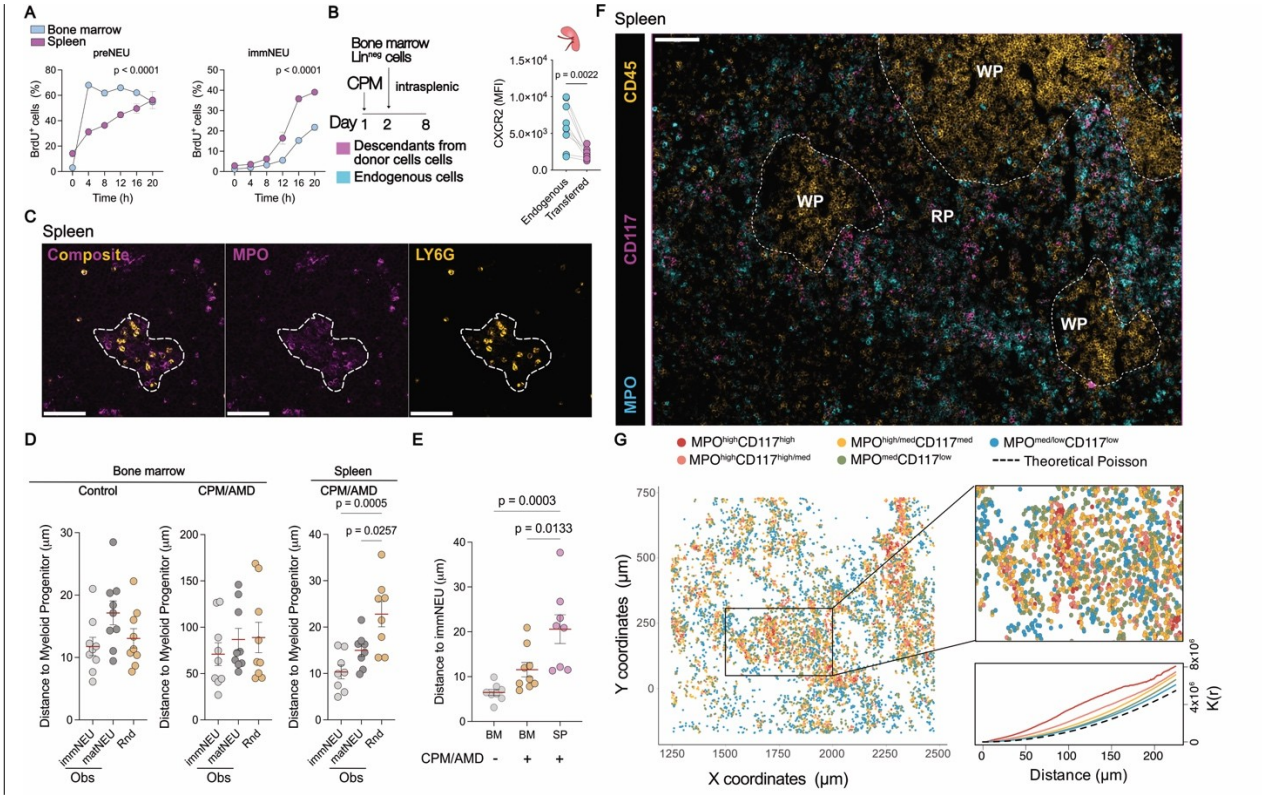

Figure 3. Accelerated differentiation of splenic neutrophils from spatially clustered progenitors. **(A)** CPM/AMD-treated mice were injected with a pulse of 5 ´Bromo-deoxyuridine (BrdU) and sacrificed at indicated time-points. Shown is the percentage of $BrdU^+$ cells. Data are mean±SEM. Two-way ANOVA with Šidák's post-hoc correction. n = 2-4 mice per group. **(B)** Mice were subjected to CPM followed by subcapsular splenic injection of $2x10^5$ lineage negative cells and sacrificed 8 days after. CXCR2 expression in donor respective to endogenous neutrophils in the spleen. **(C/D)** Immunofluorescence images depicting nuclei (DAPI, blue), Myeloperoxidase (MPO, magenta), Ly6G (ochre) in the red pulp of the spleen of CPM/AMD-treated mice. Scale bar: 100 µm. Neutrophil production cluster delineated by dashed white line. **(D/E)** Distance analysis of indicated cell subpopulations. (D) Analysis of immature ($MPO^{med}Ly6G^{med}$) and mature ($MPO^{low}Ly6G^{high}$) neutrophils to myeloid progenitors ($MPO^{high}Ly6G^{low}$). Obs: Observed; Rnd: Random. One-way ANOVA with Tukey's post-hoc correction. n = 8-9 images from 3 mice/group. Data are mean +/- SEM. (**E**) Quantification of distance (pixels) of mature neutrophils to immature neutrophils. One-way ANOVA with Tukey's post-hoc correction. n = 8-9 images from 3 mice/group. Data are mean +/- SEM. (**F**) Immunofluorescence images depicting MPO (cyan), CD117 (magenta) and CD45 (ochre) from human spleen specimen. Dashed lines delineate the white pulp (WP). RP: Red pulp. Scale bar: 100 µm. (**G**) Scatter plot showing X and Y coordinates of segmented cells with $MPO^{high}CD117^{high}$ (red), $MPO^{high}CD117^{high/med}$ (pink), $MPO^{high}CD117^{med}$ (orange), $MPO^{med}CD117^{low}$ (green), $MPO^{low}CD117^{low}$ (blue, left panel). Ripley's K function analysis of defined cell clusters (right panel).

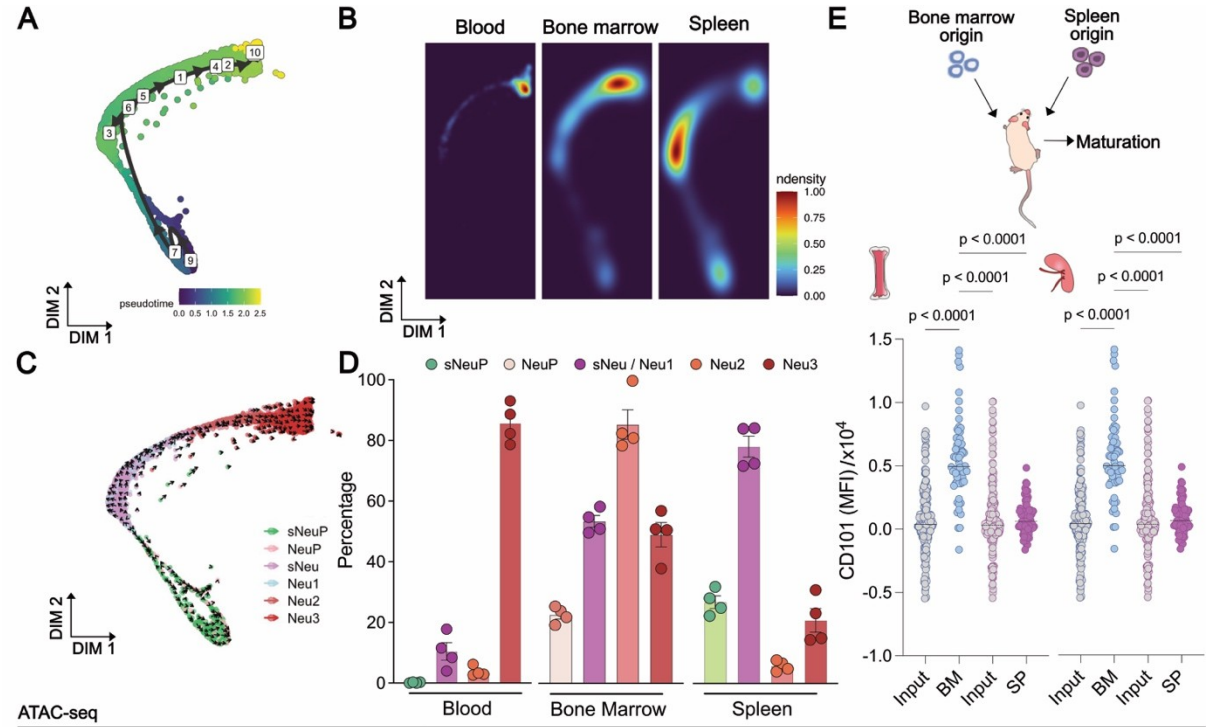
A
B
Blood
Bone marrow
Spleen
ndensity
DIM 2
DIM 1
pseudotime
C
sNeuP
NeuP
sNeu
Neu1
Neu2
Neu3
D
sNeuP
NeuP
sNeu / Neu1
Neu2
Neu3
Percentage
Blood
Bone Marrow
Spleen
E
Bone marrow origin
Spleen origin
Maturation
p < 0.0001
CD101 (MFI)/x10^4
Input
BM
SP
ATAC-seq

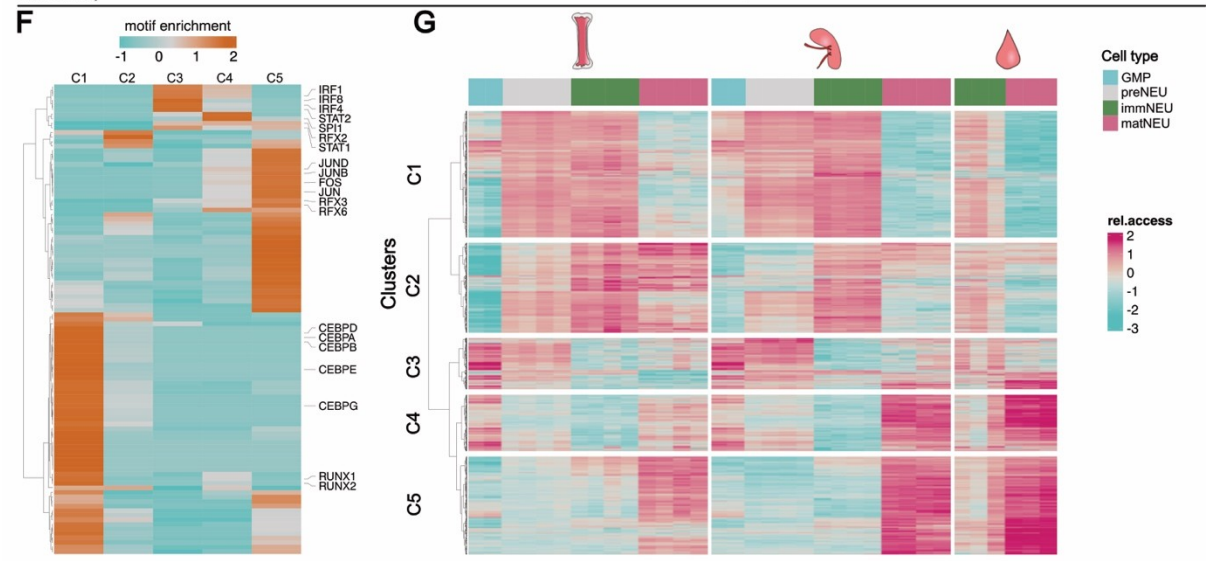
F
motif enrichment
C1
C2
C3
C4
C5
IRF1
IRF8
IRF4
STAT2
SPI1
RFX2
STAT1
JUND
JUNB
FOS
JUN
RFX3
RFX6
CEBPD
CEBPA
CEBPB
CEBPE
CEBPG
RUNX1
RUNX2
G
Cell type
GMP
preNEU
immNEU
matNEU
rel.access
Clusters

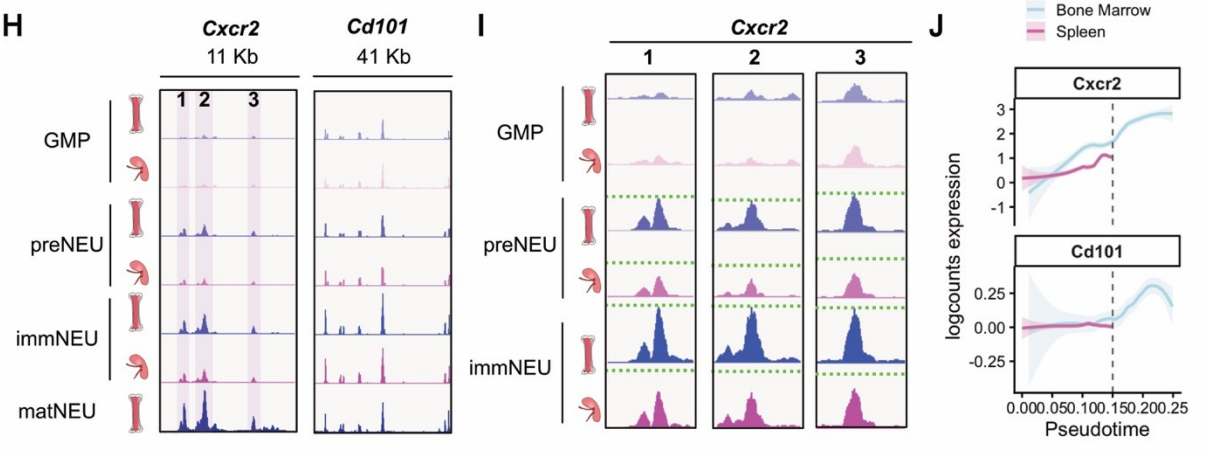
H
Cxcr2
11 Kb
Cd101
41 Kb
GMP
preNEU
immNEU
matNEU
I
Cxcr2
J
Bone Marrow
Spleen
Cxcr2
Cd101
logcounts expression
Pseudotime

Figure 4. **Epigenetic rewiring of splenic neutrophil progenitors to generate alternative granulopoiesis differentiation paths**. C57BL6/J female mice were administered with cyclophosphamide (CPM), followed by daily administration of 5 mg/kg of AMD3100 (AMD). **(A)** PAGA trajectory plot calculated on aggregated neutrophils from blood, bone marrow and spleen representing pseudotime values. Milestones represent the dynamic transition between cell states. **(B)** Density plot showing cell density across neutrophil granulopoiesis obtained from scRNA-seq analysis in blood, bone marrow and spleen from CPM/AMD-treated mice. **(C)** Velocity analysis on scRNA-seq data from aggregated neutrophils from blood, bone marrow and spleen. **(D)** Relative abundance analysis of identified clusters of indicated organs. **(E)** Immature neutrophils ($B220^{-}CD19^{-}CD3^{-}CD115^{-}F4/80^{-}SSC^{high}CXCR2^{low}$) isolated from bone marrow (dsRED) or spleen ($Lyz2^{eGFP}$) were adoptively transferred intravenously into control mice. Flow cytometry analysis of CD101 expression of donor neutrophils isolated from the recipient bone marrow or spleen. Data is represented respective to CD101 levels of input. n = 20-200 cells out of 6 mice. One-way ANOVA analysis with Tukey's correction. ****p<0.0001. **(F/G)** ATAC-seq analysis of sorted GMPs, preNEU, immNEU and matNEU from CPM/AMD-treated mice and indicated organs. (F) Heatmap showing motif enrichment analysis from unbiased clustered chromatin peaks. **(G)** Heatmap showing chromatin accessibility in indicated organs and cell types. **(H)** Chromatin accessibility for peaks associated of *Cxcr2* and *Cd101* genes in spleen vs bone marrow indicated cell types. **(I)** Close-up of *Cxcr2* peaks (indicated as 1, 2, and 3 in A) with reduced openness. Dashed line (green) defines the height of the higher peak for each cell stage in the bone marrow. **(J)** Transcriptomic expression analysis of *Cxcr2* and *Cd101* across pseudotime of splenic and bone marrow granulopoiesis.

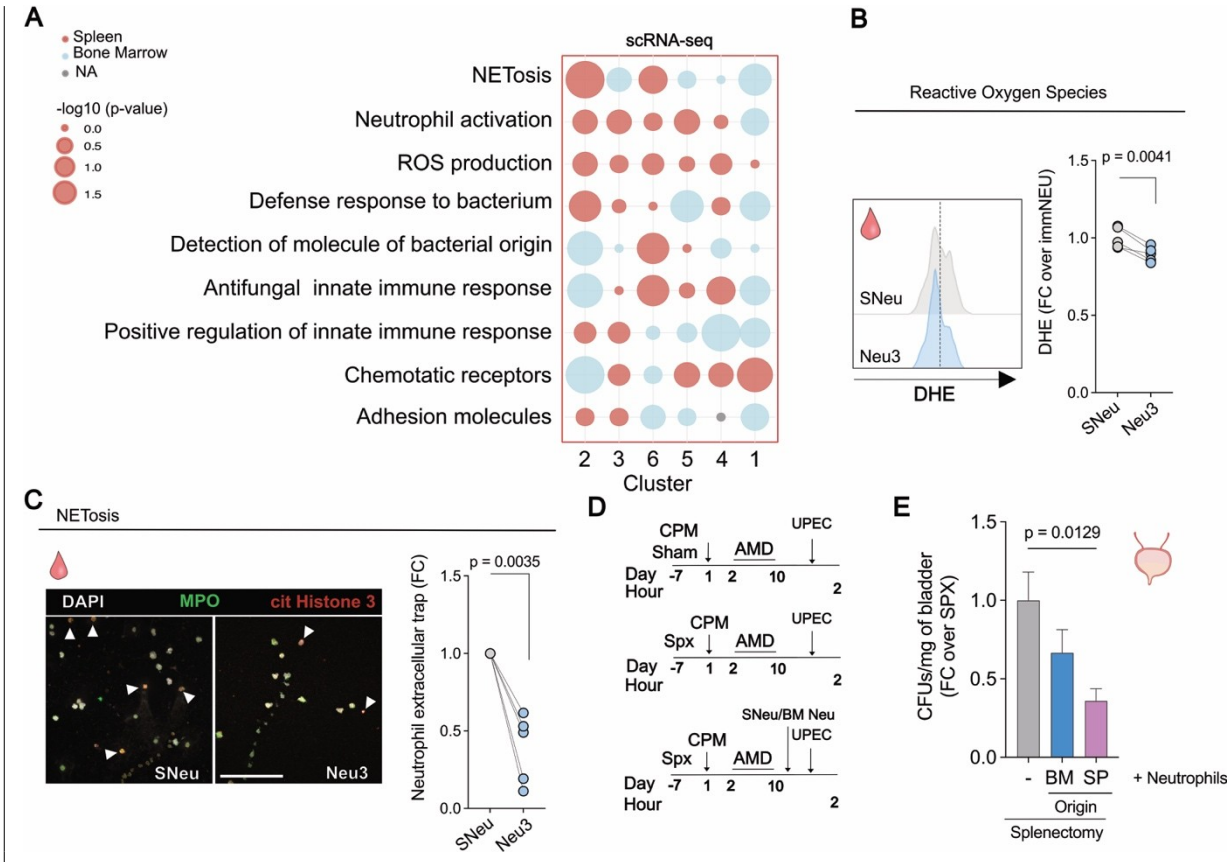

Figure 5. Splenic neutrophils facilitate bacterial clearance. C57BL6/J female mice were administered with cyclophosphamide (CPM), followed by daily administration of 5 mg/kg of AMD3100 (AMD). **(A)** Bubble plot showing the fold-change expression of indicated enriched signatures across clusters (2, 3, 6, 5, 4, 1 from immature to mature) between spleen (red) and bone marrow (blue). **(B)** Cytometry analysis of ROS using DHE in immature ($Ly6G^{+}CD101^{low}CXCR2^{low}$) or mature ($Ly6G^{+}CD101^{high}CXCR2^{high}$) blood neutrophils incubated with LPS (1 ng/mL). Two-sided paired t-test. **(C)** Confocal immunofluorescence analysis of NETs (DAPI (nuclei), MPO, citrullinated histone H3 (cit Histone H3)) in circulating neutrophils incubated with LPS (1 ng/mL). Scale bar: 100µm. Two-sided paired t-test. **(D, E)** Mice were subjected to splenectomy (Spx) or sham operated. A group of splenectomized mice was administered with SNeu or bone marrow neutrophils. All groups were infected with $5x10^{8}$ uropathogenic *E.coli* and sacrifice 4 hours post-infection. (D) Scheme of experimental procedure. (E) Bacteria colonies (colony forming units, CFU) measured in tissue bladder dissociates.

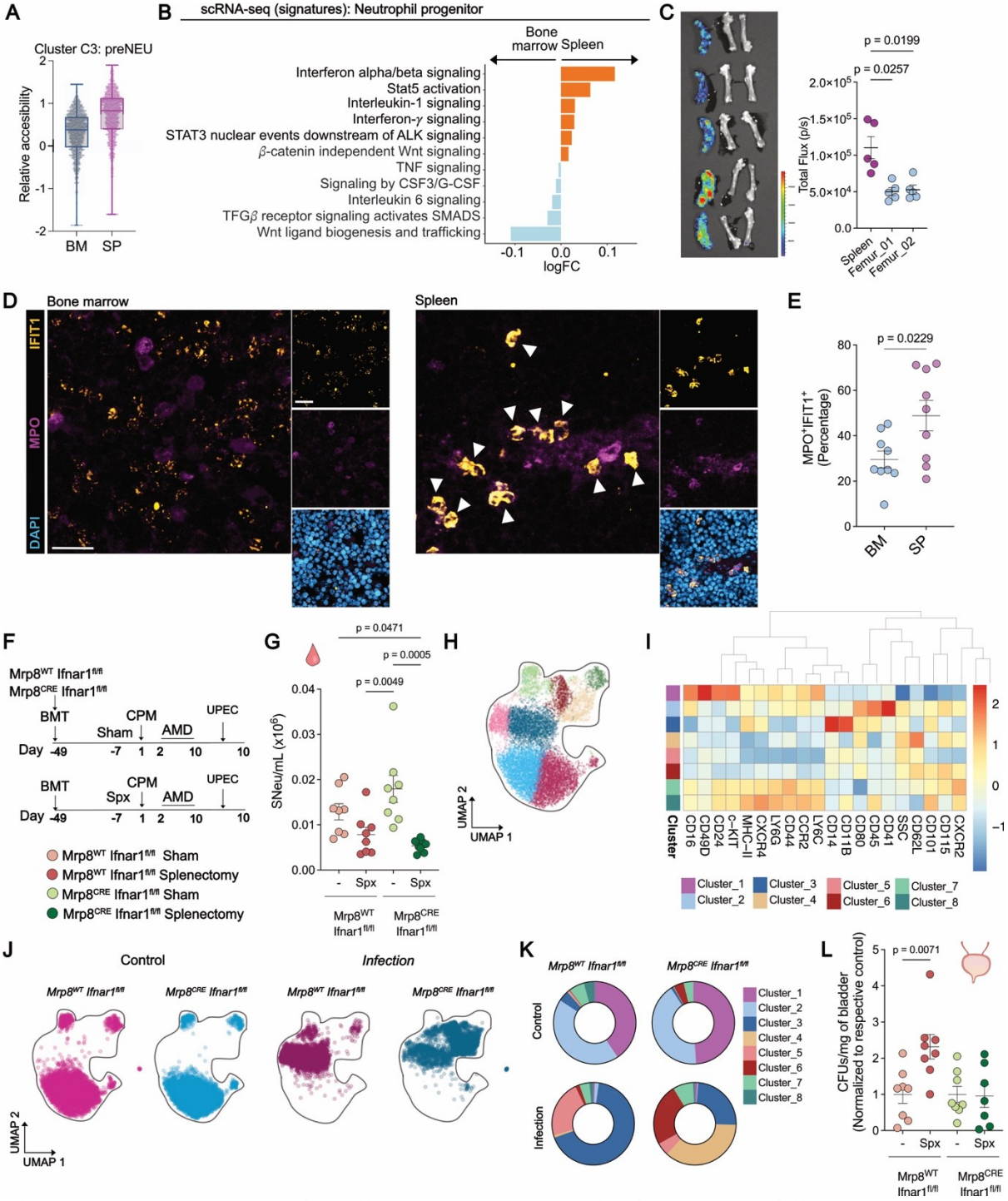

Figure 6. Interferon signaling programs splenic neutrophils for superior antimicrobial defense. **(A)** Analysis of relative accessibility peaks for cluster 3 in preNEU. **(B)** Signature enrichment analysis in neutrophil progenitor cells from spleen and bone marrow for signaling pathways. Data are mean +/- SEM. GMP: Granulocyte-Macrophage Progenitor; immNEU: immature neutrophil; matNEU: mature neutrophil. **(C)** Albino IFN-β reporter mice were treated with CPM (i.p., 4 mg per mouse) followed by 10 consecutive days of AMD3100 (s.c., 5 mg/kg). Femurs and spleens were isolated after 10 days and imaged in an IVIS Lumina Imaging System. Representative image of showing scaled luminescence photons (left) and quantification of photons per second in indicated organs (right). **(D)** Confocal immunofluorescence of bone marrow and spleen tissue of CPM/AMD-treated

C57BL6/J mice showing nuclei (DAPI, blue), Myeloperoxidase (MPO, magenta) and Interferon Induced Protein with Tetratricopeptide Repeats 1 (IFIT1, ochre). Scale bar: 20µm. **(E)** Analysis of the percentage $MPO^{+}IFIT1^{+}$ in the bone marrow and spleen. Two-sided unpaired t-test. **(F-L)** Mice were lethally irradiated and transplanted with bone marrow cells from *Mrp8*^{cre}*Ifnar1*$^{fl/fl}$ or *Mrp8*^{wt}*Ifnar1*$^{fl/fl}$. After reconstitution, mice were subjected to splenectomy or sham, followed by treatment with CPM/AMD. **(F)** Scheme of experimental procedure. **(G)** Flow cytometry analysis of immature neutrophils in blood before infection. **(H)** UMAP (calculated from expression of CD101, CD14, CD24, LY6G, CD11b, CD49d, cKIT, CD62L, CD44, CXCR4, CCR2, CXCR2, CD80, CD16, CD45) showing unbiased clustering of aggregated cells from blood neutrophils before infection. **(I)** Heatmap analysis of surface proteins in identified clusters. **(J)** UMAP showing neutrophils across indicated genotypes and conditions. **(K)** Venn diagram showing cluster proportions in indicated conditions. **(L)** Bacteria colonies (colony forming-units, CFU) measured in tissue bladder dissociates. One-way ANOVA with Tukey's correction. n = 7-8 mice/group. Data are mean +/- SEM.

References

1. L. Yvan-Charvet, L. G. Ng, Granulopoiesis and Neutrophil Homeostasis: A Metabolic, Daily Balancing Act. *Trends Immunol* 40, 598-612 (2019).
2. J. W. Swann, O. C. Olson, E. Passegue, Made to order: emergency myelopoiesis and demand-adapted innate immune cell production. *Nat Rev Immunol*, (2024).
3. N. Mende, E. Laurenti, Hematopoietic stem and progenitor cells outside the bone marrow: where, when, and why. *Exp Hematol* 104, 9-16 (2021).
4. A. Burberry *et al.*, Infection mobilizes hematopoietic stem cells through cooperative NOD-like receptor and Toll-like receptor signaling. *Cell Host Microbe* 15, 779-791 (2014).
5. P. Dutta *et al.*, Macrophages retain hematopoietic stem cells in the spleen via VCAM-1. *J Exp Med* 212, 497-512 (2015).
6. F. Leuschner *et al.*, Rapid monocyte kinetics in acute myocardial infarction are sustained by extramedullary monocytopoiesis. *J Exp Med* 209, 123-137 (2012).
7. C. S. Robbins *et al.*, Extramedullary hematopoiesis generates Ly-6C(high) monocytes that infiltrate atherosclerotic lesions. *Circulation* 125, 364-374 (2012).
8. C. Wu *et al.*, Spleen mediates a distinct hematopoietic progenitor response supporting tumor-promoting myelopoiesis. *J Clin Invest* 128, 3425-3438 (2018).
9. X. Xie *et al.*, Single-cell transcriptome profiling reveals neutrophil heterogeneity in homeostasis and infection. *Nat Immunol* 21, 1119-1133 (2020).
10. C. N. Inra *et al.*, A perisinusoidal niche for extramedullary haematopoiesis in the spleen. *Nature* 527, 466-471 (2015).
11. K. R. Moon *et al.*, Visualizing structure and transitions in high-dimensional biological data. *Nat Biotechnol* 37, 1482-1492 (2019).
12. M. Casanova-Acebes *et al.*, Rhythmic modulation of the hematopoietic niche through neutrophil clearance. *Cell* 153, 1025-1035 (2013).
13. I. Ballesteros *et al.*, Co-option of Neutrophil Fates by Tissue Environments. *Cell* 183, 1282-1297 e1218 (2020).
14. M. Casanova-Acebes *et al.*, Neutrophils instruct homeostatic and pathological states in naive tissues. *J Exp Med* 215, 2778-2795 (2018).
15. S. Pontes-Quero *et al.*, Dual ifgMosaic: A Versatile Method for Multispectral and Combinatorial Mosaic Gene-Function Analysis. *Cell* 170, 800-814 e818 (2017).
16. A. Herault *et al.*, Myeloid progenitor cluster formation drives emergency and leukaemic myelopoiesis. *Nature* 544, 53-58 (2017).
17. Q. Wu *et al.*, Resilient anatomy and local plasticity of naive and stress haematopoiesis. *Nature* 627, 839-846 (2024).
18. J. Zhang *et al.*, In situ mapping identifies distinct vascular niches for myelopoiesis. *Nature* 590, 457-462 (2021).
19. T. E. Khoyratty *et al.*, Distinct transcription factor networks control neutrophil-driven inflammation. *Nat Immunol* 22, 1093-1106 (2021).
20. D. Regan-Komito *et al.*, GM-CSF drives dysregulated hematopoietic stem cell activity and pathogenic extramedullary myelopoiesis in experimental spondyloarthritis. *Nat Commun* 11, 155 (2020).
21. G. F. Weber *et al.*, Interleukin-3 amplifies acute inflammation and is a potential therapeutic target in sepsis. *Science* 347, 1260-1265 (2015).
22. M. Evrard *et al.*, Developmental Analysis of Bone Marrow Neutrophils Reveals Populations Specialized in Expansion, Trafficking, and Effector Functions. *Immunity* 48, 364-379 e368 (2018).
23. C. Silvestre-Roig, Z. G. Fridlender, M. Glogauer, P. Scapini, Neutrophil Diversity in Health and Disease. *Trends Immunol* 40, 565-583 (2019).
24. L. Kalafati *et al.*, Innate Immune Training of Granulopoiesis Promotes Anti-tumor Activity. *Cell* 183, 771-785 e712 (2020).

25. N. Khan *et al.*, beta-Glucan reprograms neutrophils to promote disease tolerance against influenza A virus. *Nat Immunol* 26, 174-187 (2025).
26. L. Schaupp *et al.*, Microbiota-Induced Type I Interferons Instruct a Poised Basal State of Dendritic Cells. *Cell* 181, 1080-1096 e1019 (2020).
27. M. G. Manz, S. Boettcher, Emergency granulopoiesis. *Nat Rev Immunol* 14, 302-314 (2014).
28. L. J. Bayne *et al.*, Tumor-derived granulocyte-macrophage colony-stimulating factor regulates myeloid inflammation and T cell immunity in pancreatic cancer. *Cancer Cell* 21, 822-835 (2012).
29. S. B. Coffelt *et al.*, IL-17-producing gammadelta T cells and neutrophils conspire to promote breast cancer metastasis. *Nature* 522, 345-348 (2015).
30. X. Li *et al.*, Maladaptive innate immune training of myelopoiesis links inflammatory comorbidities. *Cell* 185, 1709-1727 e1718 (2022).
31. S. Ohtsu *et al.*, Enhanced neutrophilic granulopoiesis in rheumatoid arthritis. Involvement of neutrophils in disease progression. *J Rheumatol* 27, 1341-1351 (2000).
32. C. Silvestre-Roig, Q. Braster, A. Ortega-Gomez, O. Soehnlein, Neutrophils as regulators of cardiovascular inflammation. *Nat Rev Cardiol* 17, 327-340 (2020).
33. Y. P. Zhu *et al.*, Identification of an Early Unipotent Neutrophil Progenitor with Pro-tumoral Activity in Mouse and Human Bone Marrow. *Cell Rep* 24, 2329-2341 e2328 (2018).
34. G. Carissimo *et al.*, Whole blood immunophenotyping uncovers immature neutrophil-to-VD2 T-cell ratio as an early marker for severe COVID-19. *Nat Commun* 11, 5243 (2020).
35. J. B. G. Mackey, S. B. Coffelt, L. M. Carlin, Neutrophil Maturity in Cancer. *Front Immunol* 10, 1912 (2019).
36. C. A. Prada-Medina, J. P. S. Peron, H. I. Nakaya, Immature neutrophil signature associated with the sexual dimorphism of systemic juvenile idiopathic arthritis. *J Leukoc Biol* 108, 1319-1327 (2020).
37. J. Schulte-Schrepping *et al.*, Severe COVID-19 Is Marked by a Dysregulated Myeloid Cell Compartment. *Cell* 182, 1419-1440 e1423 (2020).
38. A. Silvin *et al.*, Elevated Calprotectin and Abnormal Myeloid Cell Subsets Discriminate Severe from Mild COVID-19. *Cell* 182, 1401-1418 e1418 (2020).
39. M. Wan *et al.*, Immature neutrophil is associated with coronary plaque vulnerability based on optical coherence tomography analysis. *Int J Cardiol* 374, 89-93 (2023).
40. V. Cortez-Retamozo *et al.*, Origins of tumor-associated macrophages and neutrophils. *Proc Natl Acad Sci U S A* 109, 2491-2496 (2012).
41. H. Emami *et al.*, Splenic metabolic activity predicts risk of future cardiovascular events: demonstration of a cardiosplenic axis in humans. *JACC Cardiovasc Imaging* 8, 121-130 (2015).
42. E. J. Kim, S. Kim, D. O. Kang, H. S. Seo, Metabolic activity of the spleen and bone marrow in patients with acute myocardial infarction evaluated by 18f-fluorodeoxyglucose positron emission tomograpic imaging. *Circ Cardiovasc Imaging* 7, 454-460 (2014).
43. E. Coppin *et al.*, Splenic hematopoietic stem cells display a pre-activated phenotype. *Immunol Cell Biol*, (2018).
44. G. Drifte, I. Dunn-Siegrist, P. Tissieres, J. Pugin, Innate immune functions of immature neutrophils in patients with sepsis and severe systemic inflammatory response syndrome. *Crit Care Med* 41, 820-832 (2013).
45. E. van Grinsven *et al.*, Immature Neutrophils Released in Acute Inflammation Exhibit Efficient Migration despite Incomplete Segmentation of the Nucleus. *J Immunol* 202, 207-217 (2019).

46. B. E. Hsu *et al.*, Immature Low-Density Neutrophils Exhibit Metabolic Flexibility that Facilitates Breast Cancer Liver Metastasis. *Cell Rep* 27, 3902-3915 e3906 (2019).
47. C. M. Rice *et al.*, Hyperactive immature state and differential CXCR2 expression of neutrophils in severe COVID-19. *Life Sci Alliance* 6, (2023).
48. J. M. Adrover *et al.*, Programmed 'disarming' of the neutrophil proteome reduces the magnitude of inflammation. *Nat Immunol* 21, 135-144 (2020).
49. J. M. Adrover *et al.*, A Neutrophil Timer Coordinates Immune Defense and Vascular Protection. *Immunity* 50, 390-402 e310 (2019).